Surface-directed spinodal decomposition of fluids confined in a cylindrical pore

Daniya Davis and Bhaskar Sen Gupta*
Department of Physics, School of Advanced Sciences, Vellore Institute of Technology, Vellore, Tamil Nadu 632014, India

(Received 25 September 2023; accepted 21 November 2023; published 14 December 2023)

The surface-directed spinodal decomposition of a binary liquid confined inside a cylindrical pore is investigated using molecular dynamics simulations. One component of the liquid wets the pore surface while the other remains neutral. A variety of wetting conditions are studied. For the partial wetting case, after an initial period of phase separation, the domains organize themselves into pluglike structures and the system enters into a metastable state. Therefore, a complete phase separation is never achieved. Analysis of domain growth and the structure factor suggests a one-dimensional growth dynamics for the partial wetting case. As the wetting interaction is increased beyond a critical value, a transition from the pluglike to tubelike domain formation is observed, which corresponds to the full wetting morphology. Thus, a complete phase separation is achieved as the wetting species moves towards the pore surface and forms layers enclosing the nonwetting species residing around the axis of the cylinder. The coarsening dynamics of both the species are studied separately. The wetting species is found to follow a two-dimensional domain growth dynamics with a growth exponent $1/2$ in the viscous hydrodynamic regime. This was substantiated by the Porod tail of the structure factor. On the other hand, the domain grows linearly with time for the nonwetting species. This suggests that the nonwetting species behaves akin to a three-dimensional bulk system. An appropriate reasoning is presented to justify the given observations.

DOI: 10.1103/PhysRevE.108.064607

I. INTRODUCTION

The kinetics of phase separation of fluids in confinement are of high importance in scientific research [1–4] as well as in industry [5]. There are boundless applications of phase separating fluids in confinement. Especially the oil, gasoline, and natural gas extraction industries are highly reliant on these phenomena [6]. Nonetheless, many possibilities are still unexplored and plenty of questions regarding phase separation in such systems are unanswered. In this context, there is paramount importance in studying the transformation of single as well as multicomponent phase separating fluid mixtures.

When a homogeneous binary liquid system is rapidly cooled within the miscibility gap, it loses thermodynamic stability and undergoes phase separation, forming distinct regions or domains. Over time, these domains grow and evolve until a state of local equilibrium or saturation is reached [7–20]. However, a system under confinement behaves differently from its bulk counterpart due to the presence of additional factors like restriction, surface effects, and system size. For instance, under confinement, the emergence of anisotropic domain growth becomes apparent. This phenomenon primarily arises from the constraints imposed by the limited capacity of particles that can occupy a confined space. The salient features of phase separation in such systems are metastability and lack of observable macroscopic phase separation. In real experiments, physical systems are often enclosed within containers or possess exposed surfaces, which typically results in a preferential attraction towards one of the species of the mixture. This selective affinity can significantly influence the rate of phase separation. This phenomenon, referred to as the wetting effect, entails a continual and persistent competition between phase separation and interactions with the surface or wall.

The coarsening process is always affected by the nature of the system. Usually a single time-dependent length scale $\ell(t)$ characterizes the domain morphology [21]. This is obtained from the equal-time correlation function $C(\vec{r}, t)$, where $\vec{r}$ is the distance between two spatial points and t is the time after quench. The average domain size of the system follows the power law $\ell(t) \sim t^{\alpha}$, where α is the growth exponent. The value of α is determined by the corresponding coarsening mechanism that drives the phase separation.

For the phase separation in solid-solid and liquid-liquid mixtures, diffusion takes precedence, and the growth exponent is $\alpha = 1/3$ [22]. However, in fluid systems, the hydrodynamic effect becomes significant and the growth exponents change accordingly. In fluid-fluid mixtures the diffusive phase is short lived and the system quickly transits to the hydrodynamic regime. Here, we have two exponents corresponding to the viscous hydrodynamics ($\alpha = 1$) and inertial hydrodynamics ($\alpha = 2/3$). The results mentioned above refer to bulk systems [8,9].The process of spinodal decomposition in binary fluids within bulk systems has been extensively examined, and the principles governing their growth behaviors are comprehensively understood. [19–21].

For the phase separation of fluids in confined geometry, existing studies predominantly employ two primary methods of analysis. The first one involves utilization of the random pore Ising model [3,4,23], which maps the system onto a

*bhaskar.sengupta@vit.ac.in

network of random pores. The second method, known as the single pore model [24] is a widely accepted model for studying phase separation of liquids inside porous media, and does not rely on mapping to any specific model or randomness. For the latter, theoretical studies were conducted, focusing on the wetting behavior of a binary fluid system inside a cylindrical pore [24]. This study introduced the benchmark single pore model, which allowed one to examine the phase separation in confined space, and is particularly applicable to scenarios such as binary fluid segregation within Vycor glasses where the random pore Ising model is not suitable due to low porosity. The transition of the liquid structure from a pluglike to a tubelike form was illustrated via a wetting phase diagram. In between, there existed an intermediate capsulelike structure, which occurred only when the radius of the pore was relatively larger. The domain growth was found to slow down when it became comparable to the pore size.

The phase separation of binary liquid inside a two-dimensional porous media was studied by numerically integrating the Cahn-Hilliard equation with and without wetting effects [25]. While the random field Ising model failed to explain the slowing down of the domain growth and the breakdown of scaling laws in such systems, the single pore model successfully explained the source of slow growth. Subsequent work on a binary liquid inside a two-dimensional strip geometry involving the numerical study of the Cahn-Hilliard-Cook equation [26] further confirmed the validity of the single pore model. Later on, this work was extended to study the effect of a variety of asymmetric pores, i.e., a simple strip pore, an uneven single pore, and a junction made out of two pores [27]. The single pore method was explored further to study the liquid-liquid phase separation using molecular dynamics simulations with neutral pore wall (no wetting) [28,29].

The surface-directed spinodal decomposition in a binary liquid mixture was studied in the bulk system using a mesoscopic-level modeling in terms of coupled Vlasov-Boltzmann equations with long range interactions [30]. The effects of weak and strong surface fields on the domain growth were analyzed. A two-dimensional study on how the wetting effect on the mobile and immobile particles in the binary fluid system affects the phase separation of the latter was done in Ref. [31]. Similarly, wetting dynamics was studied in a binary Lennard-Jones system confined within planes. Attention was paid to the growth of bulk domain size and the wetting layer. The standard diffusive growth with time ($t^{1/3}$) was observed at an early stage, followed by a crossover to a linear growth [32]. Recently molecular dynamics simulation was carried out on the binary fluid inside a cylindrical nanopore with neutral wall, and the growth nature of the domain was studied before the system attained a metastable state [33]. An early time diffusive growth was observed and the later time growth exponent was found to match with the inertial hydrodynamic growth in the two-dimensional bulk system.

However, the evolution of domains of segregating fluids inside the single pore cylindrical tube in the presence of wetting interaction of a preferred component of the liquid with the confining wall has not been addressed properly till now. In particular, the effect on the domain structures and the growth laws when the wetting interaction is systematically changed is missing. As previously mentioned, this model becomes more representative of experimental observations when the influence of wetting effects is taken into account. In this paper we use extensive molecular dynamic simulation to study the kinetics of persistent interplay between the phase separation and wetting, deep within the coexistence curve.

II. MODELS AND METHODS

In this study we use a binary AB liquid mixture confined inside a cylindrical pore using molecular dynamic simulation. The fluid particles interact with each other via the Lennard-Jones (LJ) potential

$$U_{\alpha\beta}(r) = 4\epsilon_{\alpha\beta}\left[\left(\frac{\sigma_{\alpha\beta}}{r_{ij}}\right)^{12} - \left(\frac{\sigma_{\alpha\beta}}{r_{ij}}\right)^{6}\right], \tag{1}$$

where ϵ is the interaction strength, σ is the particle diameter, $r_{ij} = |r_i - r_j|$ is the scalar distance between the two particles i and j, and $\alpha, \beta \in$ A,B. The phase separation between the two types of particles is assured by assigning the interparticle diameters as $\sigma_{AA} = \sigma_{BB} = \sigma_{AB} = 1.0$ and the interaction parameters as $\epsilon_{AA} = \epsilon_{BB} = 2\epsilon_{AB} = \epsilon$. This method can be mapped to the Ising model. The computational load is reduced by assigning a cutoff at $r = r_c = 2.5$ for the LJ potential. This cutoff introduces a discontinuity in the potential and force terms. This is resolved by modifying the potential as

$$u(r) = U(r) - U(r_c) - (r - r_c)\left(\frac{dU}{dr}\right)\Big|_{r=r_c}. \tag{2}$$

The final term in the Eq. (2) avoids the abrupt jumps in the force at r_c. The system mentioned above is characterized in bulk with a critical temperature of $T_c = 1.421$ and critical density of $\rho_c = N/V = 1$ in three dimensions [34]. Here N is the number of particles in the system and V is the volume. We measure the temperature and length in units of ϵ/k_B and σ respectively. For convenience ϵ, k_B, and mass of each particle m are set to unity.

A cylindrical tube with a large length to diameter ratio is considered, which serves as a confining structure containing the binary mixture. The axis of the cylinder is chosen to be the x axis. A periodic boundary condition is applied along the length of the cylinder. The wall of the cylinder is constructed with closely packed particles similar to the fluid particles. The wetting effect is incorporated by introducing a preferable attraction of one type of particles, say type A, towards the wall via the LJ potential given in Eq. (2), and no interaction at all for the other species. The interaction between the wall and type A particles, denoted as ϵ_w is tuned over a wide range of values and the effect of this wetting strength on the phase separation is studied. We vary the ϵ_w in the range of (0.1, 0.8).

Molecular dynamics (MD) simulations are performed in the canonical ensemble. Since our system is in the liquid state, it is important to take into consideration the effect of hydrodynamics. Therefore, Nosé-Hoover thermostat is used which controls the temperature and at the same time preserves the hydrodynamics of the system [35]. The velocity-Verlet algorithm is used in the MD simulation to compute the positions and velocities of the particles with time step of $\Delta t = 0.005$ [36]. Here time is measured in units of $(m\sigma^2/\epsilon)^{1/2}$.

The cylindrical pore we consider has a radius $R = 10$ and length $L = 200$. It is filled with the binary liquid of number density $\rho = 0.8$, where 50% of the particles are type A and 50% type B. The system is first equilibrated at a high temperature of $T_i = 10$ to prepare a homogeneous mixture and then suddenly quenched to a temperature $T_f = 0.8$ well below T_c. Finally, the time evolution of the system towards the thermodynamically favored state at $T_f = 0.8$ is studied. The results are averaged over 80 independent initial configurations.

To study the domain growth and coarsening dynamics of the segregating liquid inside the cylindrical pore, we use the so-called two-point equal-time correlation function $C(\vec{r}, t)$ given by

$$C(\vec{r}, t) = \langle \psi(0, t)\psi(\vec{r}, t)\rangle - \langle \psi(0, t)\rangle\langle \psi(\vec{r}, t)\rangle. \quad (3)$$

The angular brackets represent ensemble averaging. $\psi(\vec{r}, t)$ is the order parameter of the system defined in terms of the local density fluctuations as

$$\psi(\vec{r}, t) = \frac{\rho_A(\vec{r}, t) - \rho_B(\vec{r}, t)}{\rho_A(\vec{r}, t) + \rho_B(\vec{r}, t)}. \quad (4)$$

Here $\rho_A(\vec{r}, t)$ and $\rho_B(\vec{r}, t)$ are the local concentrations of A and B particles at time t around the position $\vec{r}$. For the domain structure related studies, we resort to the static structure factor $S(\vec{k}, t)$, obtained from the Fourier transformation of the correlation function given by

$$S(\vec{k}, t) = \int d\vec{r} \exp(i\vec{k} \cdot \vec{r})\, C(\vec{r}, t), \quad (5)$$

where k is the wave vector [21]. The standard FFTW algorithm is used to compute the Fourier transformation. For the large-k limit in d dimensions, $S(\vec{k}, t)$ follows the Porod law given by

$$S(k, t) \sim k^{-(d+1)}. \quad (6)$$

A detailed description of computing the order parameter $\psi(\vec{r}, t)$ under different wetting conditions is provided in the next section.

III. RESULTS

It is well established that in a bulk system, when our symmetric binary liquid is quenched below the critical temperature, it completely phase separates into two domains of type A and type B. But when the same liquid is considered inside a cylindrical pore, after the sudden quench, phase segregation commences with the growth of tiny isotropic domains. With time, these domains grow and organize themselves into stripes along the axis of the cylinder in a periodic pattern. Therefore, pluglike domains are formed in the absence of wetting interactions between the cylinder wall and the fluid particles [24,33]. Finally, the system attains a metastable state and a complete macroscopic phase separation is never achieved. The scenario remains the same far inside the coexistence region also. The width of these domains is found to be insensitive to the length of the cylinder but varies linearly with the pore diameter.

Nevertheless, when the wetting effect is considered, the growth behavior is quite tangled. In our present study, we analyze the wetting effect on the domain growth dynamics over a wide range of wetting strengths ϵ_w, from partial to full wetting, systematically. The preferential attraction of type A particles implies that they have comparatively lesser surface tension γ_A with the wall than those of the other type, γ_B [37]. Hence, if θ is the contact angle between the fluid and wall interface, then according to Young's condition [38] $\gamma_{AB} \cos\theta = \gamma_B - \gamma_A$, where γ_{AB} is the surface tension between the A and B interface. The conditions for partial wetting and complete wetting are deduced from this criterion [37]. When $\gamma_B - \gamma_A < \gamma_{AB}$, both A and B species are in contact with the surface and the system is only partially wet. On the other hand, when $\gamma_B - \gamma_A > \gamma_{AB}$, Young's condition is not valid and the B phase is expelled from the wall resulting in the complete wetting of the wall with phase A.

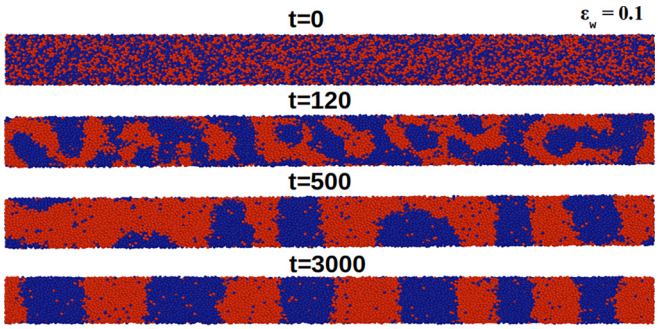

FIG. 1. The time evolution of the segregating binary liquid mixture confined inside a cylindrical pore for the partial wetting interaction $\epsilon_w = 0.1$. Here we show the orthogonal view of the cylinder. A and B types of particles are represented by red and blue colors respectively.

Following the rapid cooling process, the phase segregation begins as small isotropic domains starts to form inside the pore. The interaction of phase separation and wetting, known as surface-directed spinodal decomposition, involves a dynamic interplay between these two kinetic processes. In Fig. 1 we show the time evolution of the domain structures of our system for the wetting interaction $\epsilon_w = 0.1$. The outcome is more or less close to the phase separation of the binary liquid inside the nanopore without wetting [26,33]. The system freezes into a multidomain metastable state and no further domain evolution is observed with time. This outcome can be attributed to the following. When the adjacent stripes are separated by more than a characteristic distance, the length scale saturates as a result of a weak contact between the fronts of the neighboring stripes. The pluglike structures are formed and the metastable state is reached.

In Fig. 2 we show the domain structures corresponding to the longest possible simulation time for the wetting interactions ϵ_w in the range 0.1 to 0.5. It clearly depicts how the metastable state varies with ϵ_w. The width of the striped domains appears to increase as the wetting strength increases. This is because the pore wall acts as a bridge between the alternative stripes, which facilitates phase separation with increasing ϵ_w. We find a critical field strength $\epsilon_w = 0.5$ up to which the metastable phase separation takes place with the formation of stripes. Therefore, $\epsilon_w \leqslant 0.5$ corresponds to partial wetting.

As the wetting strength is increased further, stripe formation no longer occurs. Instead, the transition from a pluglike to

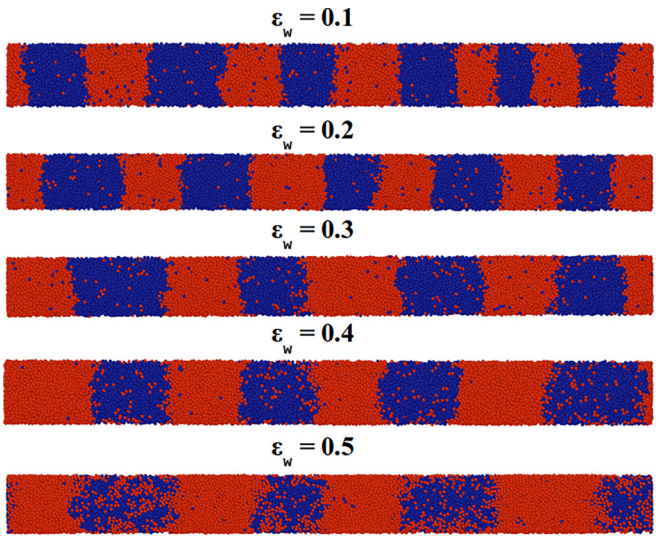

FIG. 2. Final configurations of our binary liquid system forming plug like domain structure for different wetting interactions ϵ_w. Here we show the orthogonal view of the cylinder. A and B types of particles are represented by red and blue colors respectively.

a tubelike domain is observed, which corresponds to the full wetting morphology. In Fig. 3 we show the time evolution of the domain structure for the highest interaction strength $\epsilon_w = 0.8$ chosen in our simulation. We clearly observe a complete phase separation of the binary liquid inside the pore. For better visualization, the cross sectional view of the system after the complete phase separation is shown in Fig. 4. This surface field value satisfies the complete wetting condition mentioned above. Correspondingly, the type A particles interact with the pore wall, forming a layer near it. On the other hand, the neutral B type particles are pushed towards the axis of the cylinder [24]. Thus our simulation confirms that, when the wetting interaction is above a particular threshold value (in our

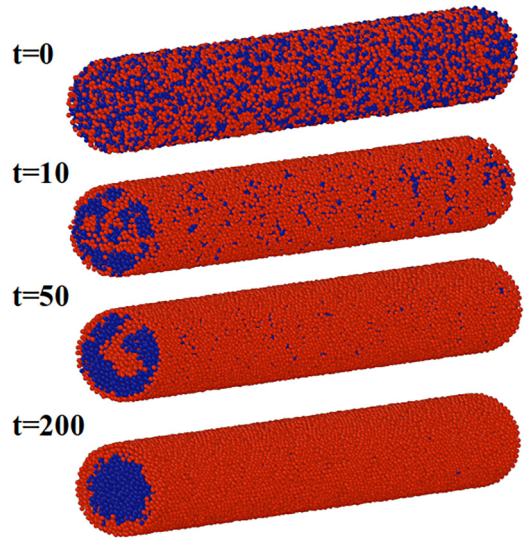

FIG. 3. Representative snapshots for the phase separating binary liquid mixture inside the cylindrical pore for the full wetting interaction $\epsilon_w = 0.8$.

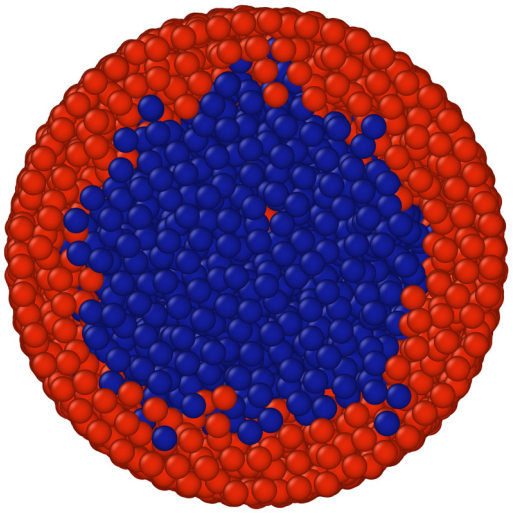

FIG. 4. The cross sectional view of the fully phase separated liquid inside the pore.

case $\epsilon_w > 0.5$), we find the tubelike domain along the axis of the cylinder formed by the nonwetting particles, whereas the wetting species coats the inner surface of the pore. Therefore, a complete phase separation is achieved for the full wetting case.

Next, we examine the dynamical properties of the system for the partial wetting case, that exhibits stripe formation. Since the geometrical confinement imposed on the system results in the stripe patterned domains, growth is analyzed along the axial direction [28,29]. Therefore, the order parameter takes the form

$$\psi(x,t) = \frac{\rho_A(x,t) - \rho_B(x,t)}{\rho_A(x,t) + \rho_B(x,t)}. \tag{7}$$

To compute $\psi(x,t)$ we divide the cylinder vertically into sections of equal width $\Delta x = 2.0$. $\rho_A(x,t)$ and $\rho_B(x,t)$ are calculated for each section and thus $\psi(x,t)$ is obtained from Eq. (7).

To study the domain growth dynamics we compute the two-point equal-time correlation function given by Eq. (3) along the x axis. For the wetting strength $\epsilon_w \leqslant 0.5$, the observation of a consistent self-similarity pattern in stripe formation suggests that our system is likely to adhere to the scaling law $C(x,t) \equiv \tilde{C}(x/\ell(t))$, where $\tilde{C}$ is a time-independent master scaling function [21]. The identification of this scaling law enables the definition of a time-dependent length scale $\ell(t)$ based on the decay of $C(x,t)$. Throughout the paper, we utilize the first zero-crossing of $C(x,t)$ as a reliable measure of $\ell(t)$

Figure 5 confirms the scaling law of the correlation where $C(x,t)$ is plotted vs $x/\ell(t)$ for different strengths of wall interactions corresponding to partial wetting at a given time. The data collapse is highly evident, except for the case of $\epsilon_w = 0.5$, where the impact of wetting is close to disrupting the barrier responsible for stripe formation and maintaining a metastable equilibrium. So, we can generalize that the Porod law is valid for partial wetting. Note that the scaling holds well for $x/\ell(t) < 1$. The violation of the scaling law beyond this point can be comprehended as follows. The $x/\ell(t) = 1$

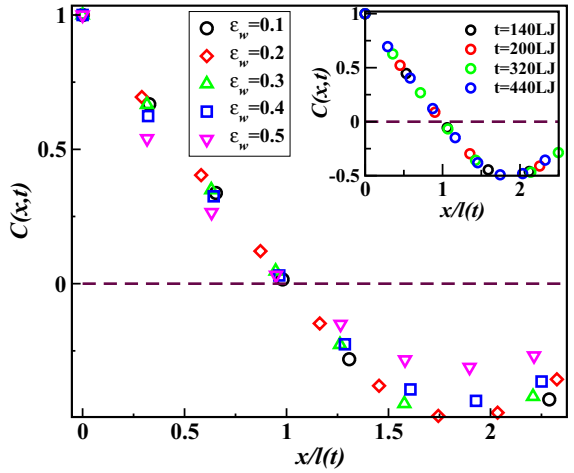

FIG. 5. Scaled correlation function $C(x,t)$ vs $x/\ell(t)$ for different partial wetting interactions ϵ_w at a fixed time $t = 320$. In the inset we show the scaling plot of $C(x,t)$ vs $x/\ell(t)$ for $\epsilon_w = 0.2$ for different times.

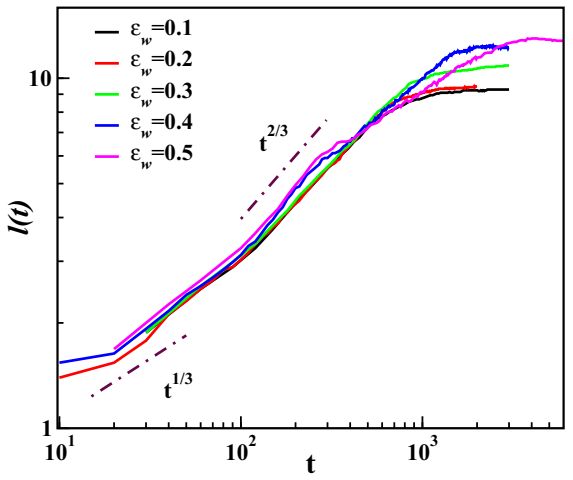

FIG. 7. The time evolution of the length scale $\ell(t)$ for the partial wetting case with different ϵ_w. The dashed lines are the reference for the power law growth.

corresponds to the domain interface between two successive stripes. For $x/l(t) > 1$, the domain boundary is crossed and the correlation becomes negative. The results indicate that within a stripe the domain morphology is self-similar in nature. Once the interface is crossed, the self-similarity is lost for different ϵ_w values and the correlation curves do not overlap. The inset of the figure shows the scaling of correlation for a particular choice of $\epsilon_w = 0.2$ at different times. We observe an excellent data collapse. A similar scaling behavior is observed for other ϵ_w values also (not shown here).

To examine patterns and investigate domain structures in both simulations and experiments, it is a common practice to calculate the structure factor. One-dimensional correspondence of Eq. (5) is used for this purpose. Figure 6 shows the scaled structure factor. The decaying part of the tail exhibits a power law $S(k,t) \sim k^{-2}$, showing the Porod law behavior and supporting the one-dimensional growth in the system as defined in Eq. (6). Additionally, the $S(k,t) \sim k^2$

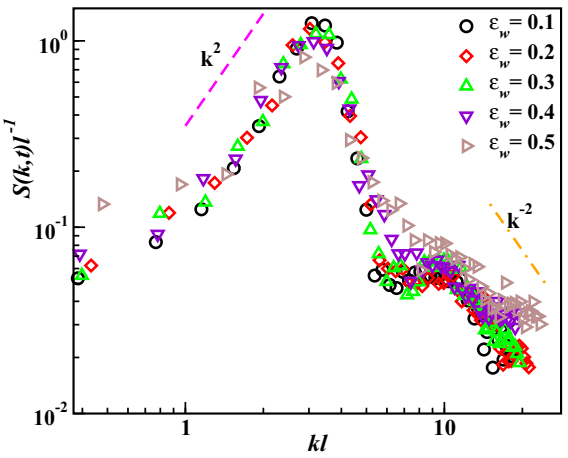

FIG. 6. The scaled structure factor $S(k,t)\ell^{-1}$ vs $k\ell$ for the different partial wetting strengths ϵ_w. The dashed lines are guide lines for the Porod law.

behavior at the small-k limit further supports the argument of one-dimensional domain growth. The second peak at $kl \sim 10$ corresponds to the sharp interface between two successive stripes. Note that, for smaller $\epsilon_w = 0.1$, 0.2, and 0.3, the stripes are clearly formed with sharp interfaces. With further increase of ϵ_w, we approach the critical wetting strength for the transition from partial to full wetting, where the stripe interfaces are rough and less distinct and the cylindrical domains start to form. Consequently, for $\epsilon_w = 0.4$ and 0.5, which are in proximity to the critical transition value, an anticipated deviation of the structure factor from the one-dimensional Porod law is expected due to this morphological transition.

The correlation and structure factor clearly show an onset of deviation for $\epsilon_w = 0.5$, as they start to diverge from the one-dimensional growth and the wetting effect becomes dominant and tends to shift towards the capsulelike structure. The pore diameter not being large enough, we do not observe a proper capsule formation. Instead, a direct transition occurs from plug- to tubelike domains as ϵ_w is increased further. A more detailed discussion of this phenomenon will follow.

Subsequently, our attention turns to quantifying the growth of the stripes along the axial direction in terms of the length scale $\ell(t)$. As mentioned earlier, this quantity is computed from the first zero crossing of the correlation function $C(x = \ell, t) = 0$. The time evolution of $\ell(t)$ is shown in Fig. 7. The dashed lines in the graph show the power law correspondence at different stages of the growth. The transport mechanism in the system decides the rate of domain growth. During the initial stage, the system exhibits diffusive behavior, following the Lifshitz-Slyozov growth law as $t^{1/3}$. The slight deviation can be attributed to the finite system size effect. When a homogeneous system equilibrated at high temperature is quenched suddenly below T_C at time $t = 0$, it becomes unstable because of fluctuations. Usually at this stage the domain growth is quantified by the equation $\ell(t) = \ell_0 + At^{\alpha}$ [39], where ℓ_0 is the average cluster size immediately after quench at $t = 0$. A specific domain size interpretation is not attributed to this parameter. Instead, it is regarded in a manner analogous to a background quantity encountered in critical phenomena. Such

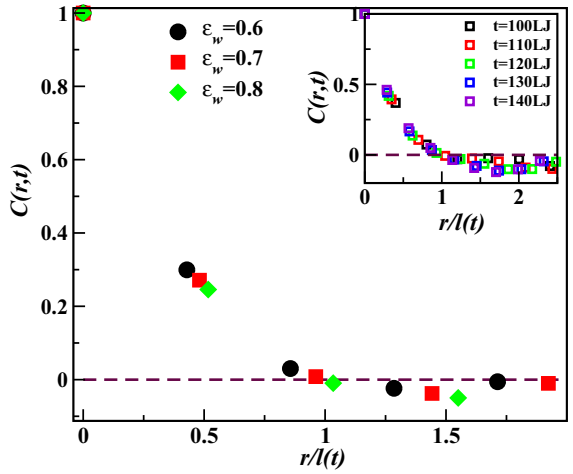

FIG. 8. Scaled correlation function $C(r,t)$ vs $r/\ell(t)$ for different ϵ_w corresponding to the full wetting case. In the inset we show the scaling plot of $C(r,t)$ vs $r/\ell(t)$ for $\epsilon_w = 0.8$ for different times. Both the graphs correspond to type A particles.

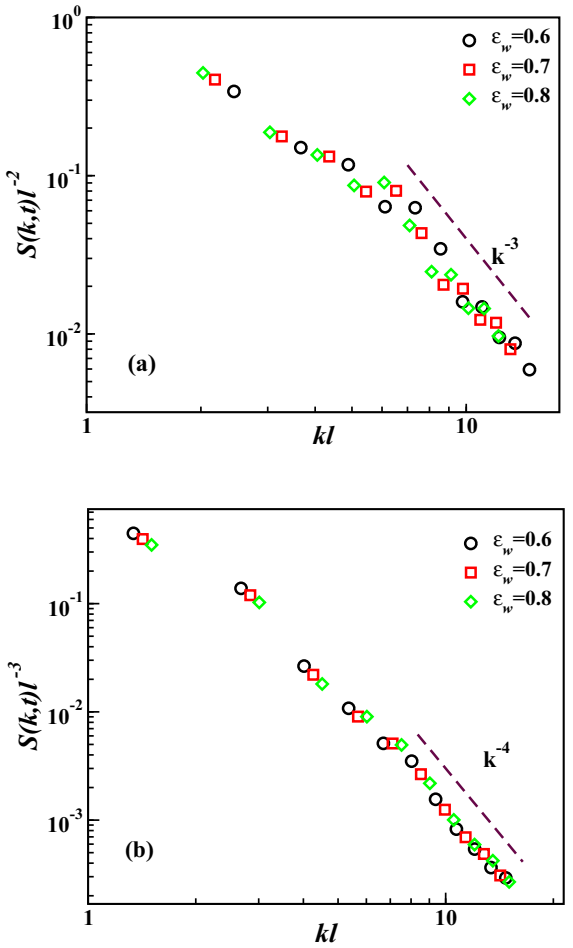

FIG. 9. The scaled structure factor $S(k,t)\ell^{-1}$ vs $k\ell$ graph for different ϵ_w corresponding to the full wetting case at a fixed time $t = 110$ for the (a) wetting species (A particles) and (b) nonwetting species (B particles). The dashed lines are guide lines for the Porod law.

background quantities arise from minor length fluctuations, and their temperature-dependent variations are typically disregarded. The term At^{α} stands for the scaling of domain growth. For large system size, $\ell(t) \gg \ell_0$. Nonetheless, in computer simulations involving small systems, ℓ_0 becomes comparable with $\ell(t)$ at shorter time, and therefore, the exponent α deviates from $1/3$. This is followed by a crossover to the inertial hydrodynamic growth characterized by a power law of $t^{2/3}$ [40]. The same growth exponents were obtained when the pore wall was considered neutral (nonwetting). It is worth noting that the wetting strength of $\epsilon_w = 0.5$ is evidently a critical scenario where, despite the presence of stripe domains, the dynamical properties deviate significantly from the typical behavior observed for the partial wetting case.

Next, we shift our attention to investigate the phase separation dynamics for the full wetting case, i.e., $\epsilon_w > 0.5$. A complete phase separation is achieved here via the formation of tubelike domains. A typical domain morphology is displayed in Fig. 3. It is crucial to emphasize that, during the phase separation of domains inside the pore for the complete wetting case, the correlation is assessed radially rather than axially. Hence the order parameter is calculated accordingly from Eq. (4). For that, the whole system is divided into small cubic boxes of size $(2\sigma)^3$ and the local density fluctuations are computed over these boxes. Finally, we calculate the correlation function along the radial direction from Eq. (3).

During the coarsening process, the two species proceed individually following the surface-directed spinodal decomposition. The wetting species endures surface enrichment while the other is expelled from the surface. This results in complete phase separation, as shown in Fig. 3. The correlation function for both the species is calculated separately to study their individual domain growth. Figure 8 corresponds to the scaled correlation of wetting particles. We observe a satisfactory data collapse for different interaction strengths ϵ_w. The inset shows the scaled correlation for the maximum interaction strength $\epsilon_w = 0.8$ at different times. They exhibit a perfect data collapse as well. Hence, the surface-directed migration of particles in our confined system perseveres and upholds the presence of superuniversality and the Porod law [41–43]. The same exercise is repeated for the nonwetting species (not shown), and a similar scaling behavior is observed.

Considering the rationale mentioned earlier, it is prudent to compute the structure factor independently for each of the species. The results are shown in Fig. 9 for three different ϵ_w at a particular time $t = 110$. The dotted lines correspond to the power law reference. The results clearly demonstrate that the trailing section of the structure factor exhibits distinct power laws for the two species. According to Eq. (6), wherein d represents the dimension of the domain, k^{-3} pertains to growth in two dimensions while k^{-4} refers to growth in three dimensions. This suggests that the wetting species experiences two-dimensional domain growth, while the other undergoes three-dimensional growth. This can be clearly understood from Figs. 3 and 4, where the type A particles form a layer on the inner surface of the pore wall, resembling a curved two-dimensional plane. Therefore, the structure obtained for the wetting particles is two dimensional, providing a rationale for the Porod law exponent. On the other hand, type B particles

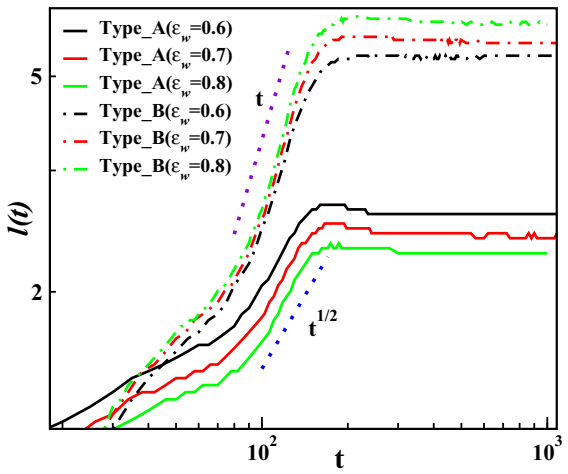

FIG. 10. The time evolution of the length scale $\ell(t)$ for the full wetting case with different ϵ_w. The solid lines and dashed dotted lines refer to the wetting and nonwetting species respectively. The dotted lines represent the power law growth.

that congregate around the axis of the cylindrical pore behave akin to a bulk system. This three-dimensional structure of the nonwetting particles is affirmed by the Porod tail behavior observed in the structure factor.

The time dependence of the characteristic domain growth for the two types of particles are computed separately for three different ϵ_w. In Fig. 10 we show $\ell(t)$ for both species. The dotted lines indicate the power law. The domain growth of the nonwetting species resembles liquids in a three-dimensional bulk system. After an initial transition period, the domain size grows as $\ell(t) \sim t$, which corresponds to the bulk viscous hydrodynamics growth. This result is consistent with the structure factor, which shows a three-dimensional Porod tail of k^{-4}.

For the wetting species, the growth law is found to be $t^{1/2}$, which resembles domain growth of liquids in a two-dimensional surface. This can be comprehended as follows. The wetting particles interact with the pore wall and form layers inside the wall, which specifically encloses the nonwetting particles. Therefore, this structure is identical to a two-dimensional curved surface. It is well known that a binary liquid phase separates with a growth law exponent of $1/2$ on a two-dimensional plane. Hence the domain growth of the wetting particles can be explained analogously. This is further endorsed by the structure factor in Fig. 9, which shows Porod tail behavior of k^{-3}. The same exercise was repeated by considering two additional cylindrical pores of different radii (not shown here), and the domain growth laws are found to be robust and insensitive to the pore size.

IV. CONCLUSION

In summary, we have studied the surface-directed spinodal decomposition of a segregating binary liquid mixture system confined inside a cylindrical pore using comprehensive molecular dynamics simulations. One of the species of the liquid adheres to the pore surface, whereas the other remains inert. A wide range of wetting interactions is contemplated, encompassing both partial and full wetting. For the partial wetting case, the domain structure resembles the nonwetting scenario. After the initial domain growth, phase separation is halted via formation of pluglike structures. The growth exponent of the domain is estimated to be $2/3$ which suggests one-dimensional growth dynamics. This is further confirmed from the Porod law tail of the structure factor.

The scenario changes completely as the wetting interaction is increased beyond a critical value ($\epsilon_w > 0.5$). The pluglike structure breaks down and cylindrical domains emerge for the full wetting case. Hence, a complete phase segregation is observed when the wetting substance migrates toward the pore surface and creates layers that encompass the nonwetting species located around the axis of the cylinder. The wetting substance is observed to adhere to a two-dimensional domain growth pattern, characterized by the growth exponent $\alpha = 1/2$ in the viscous hydrodynamic regime. This is supported by the Porod tail pertaining to the structure factor. On the other hand, the nonwetting species is found to experience linear domain growth over time. This implies that the nonwetting species behaves similarly to a three-dimensional bulk system. This behavior was additionally affirmed through an examination of the tail section of the structure factor. Our works provides a comprehensive understanding of the kinetics of phase separation in confined liquids under different wetting conditions. It is worth mentioning here that the critical value of the interaction strength for the partial to full wetting transition depends on the degree of confinement, and is found to increase with decreasing radius of the cylinder. Therefore, with decreasing pore size the confinement effect increases and a larger interaction strength is needed to obtain complete wetting. A detailed study in this direction will be reported elsewhere. Also, it will be interesting to extend this work where the confinement has complex topology, i.e., random porous media [44].

ACKNOWLEDGMENTS

B.S.G. acknowledges the Science and Engineering Research Board (SERB), Department of Science and Technology (DST), Government of India (Grant No. CRG/2022/009343) for financial support. D.D. acknowledges VIT for support via doctoral fellowship.

[1] F. Brochard and P. G. De Gennes, J. Phys. Lett. (Paris) **44**, 785 (1983).
[2] J. V. Maher, W. I. Goldburg, D. W. Pohl, and M. Lanz, Phys. Rev. Lett. **53**, 60 (1984).
[3] P. G. De Gennes, J. Phys. Chem. **88**, 6469 (1984).
[4] M. C. Goh, W. I. Goldburg, and C. M. Knobler, Phys. Rev. Lett. **58**, 1008 (1987).
[5] K. Kanamori, K. Nakanishi, and T. Hanada, Soft Matter **5**, 3106 (2009).
[6] N. R. Morrow, J. Pet. Technol. **42**, 1476 (1990).

[7] K. Binder, Phys. Rev. B **15**, 4425 (1977).
[8] E. D. Siggia, Phys. Rev. A **20**, 595 (1979).
[9] H. Furukawa, Phys. Rev. A **31**, 1103 (1985).
[10] M. San Miguel, M. Grant, and J. D. Gunton, Phys. Rev. A **31**, 1001 (1985).
[11] H. Tanaka, J. Chem. Phys. **103**, 2361 (1995).
[12] D. Beysens, Y. Garrabos, and D. Chatain, Europhys. Lett. **86**, 16003 (2009).
[13] R. Bhattacharyya and B. S. Gupta, Phys. Rev. E **104**, 054612 (2021).
[14] R. Bhattacharya and B. S. Gupta, arXiv:2104.06477.
[15] S. Puri and B. Dünweg, Phys. Rev. A **45**, R6977 (1992).
[16] C. Datt, S. P. Thampi, and R. Govindarajan, Phys. Rev. E **91**, 010101(R) (2015).
[17] M. Laradji, S. Toxvaerd, and O. G. Mouritsen, Phys. Rev. Lett. **77**, 2253 (1996).
[18] A. K. Thakre, W. K. den Otter, and W. J. Briels, Phys. Rev. E **77**, 011503 (2008).
[19] S. Ahmad, S. K. Das, and S. Puri, Phys. Rev. E **82**, 040107(R) (2010).
[20] S. Ahmad, S. K. Das, and S. Puri, Phys. Rev. E **85**, 031140 (2012).
[21] A. J. Bray, Adv. Phys. **51**, 481 (2002).
[22] C. Chen, W. Liu, H. Wang, and L. Zhu, RSC Adv. **6**, 102997 (2016).
[23] P. Wiltzius, S. B. Dierker, and B. S. Dennis, Phys. Rev. Lett. **62**, 804 (1989).
[24] A. J. Liu, D. J. Durian, E. Herbolzheimer, and S. A. Safran, Phys. Rev. Lett. **65**, 1897 (1990).
[25] A. Chakrabarti, Phys. Rev. Lett. **69**, 1548 (1992).
[26] A. Bhattacharya, M. Rao, and A. Chakrabarti, Phys. Rev. E **49**, 524 (1994).
[27] Z. Zhang and A. Chakrabarti, Phys. Rev. E **52**, 2736 (1995).
[28] L. D. Gelb and K. E. Gubbins, Phys. Rev. E **55**, R1290 (1997).
[29] L. D. Gelb and K. E. Gubbins, Phys. Rev. E **56**, 3185 (1997).
[30] S. Bastea, S. Puri, and J. L. Lebowitz, Phys. Rev. E **63**, 041513 (2001).
[31] T. Araki and H. Tanaka, Phys. Rev. E **73**, 061506 (2006).
[32] P. K. Jaiswal, S. Puri, and S. K. Das, Phys. Rev. E **85**, 051137 (2012).
[33] S. Basu, S. Majumder, S. Sutradhar, S. K. Das, and R. Paul, Europhys. Lett. **116**, 56003 (2016).
[34] S. K. Das, M. E. Fisher, J. V. Sengers, J. Horbach, and K. Binder, Phys. Rev. Lett. **97**, 025702 (2006).
[35] D. Frenkel and B. Smit, *Understanding Molecular Simulations: From Algorithms to Applications* (Academic, San Diego, 2002).
[36] L. Verlet, Phys. Rev. **159**, 98 (1967).
[37] J. W. Cahn, J. Chem. Phys. **66**, 3667 (1977).
[38] T. Young, Philos. Trans. R. Soc. London Ser. A **95**, 65 (1805).
[39] S. Majumder and S. K. Das, Phys. Rev. E **84**, 021110 (2011).
[40] H. Furukawa, Phys. Rev. A **36**, 2288 (1987).
[41] K. Binder, in *Phase Transformation of Materials*, edited by R. W. Cahn, P. Haasen, and E. J. Kramer, Material Science and Technology (VCH, Weinheim, 1991), Vol. 5, p. 405; *Kinetics of Phase Transitions*, edited by S. Puri and V. Wadhawan (CRC, Boca Raton, 2009).
[42] Z. W. Lai, G. F. Mazenko, and O. T. Valls, Phys. Rev. B **37**, 9481 (1988).
[43] F. Corberi, E. Lippiello, A. Mukherjee, S. Puri, and M. Zannetti, Phys. Rev. E **85**, 021141 (2012).
[44] R. Bhattacharya and B. S. Gupta, Europhys. Lett. **140**, 47002 (2022).